H-He collision-induced satellite in the Lyman alpha profile of DBA white dwarf stars

Nicole Allard, John F Kielkopf, Siyi Xu, Grégoire Guillon, Bilel Mehnen, Roberto Linguerri, Muneerah Mogren Al Mogren, Majdi Hochlaf, Ivan Hubeny

Monthly Notices
of the
ROYAL ASTRONOMICAL SOCIETY

MNRAS **494,** 868–875 (2020)
Advance Access publication 2020 March 13

doi:10.1093/mnras/staa707

H–He collision-induced satellite in the Lyman α profile of DBA white dwarf stars

Nicole F. Allard,[1,2]★ John F. Kielkopf,[3]★ Siyi Xu,[4]★ Grégoire Guillon,[5] Bilel Mehnen,[6] Roberto Linguerri,[6] Muneerah Mogren Al Mogren,[7] Majdi Hochlaf[6] and Ivan Hubeny[8]

[1]*GEPI, Observatoire de Paris, Université PSL, CNRS, UMR 8111, 61 Avenue de l'Observatoire, F-75014 Paris, France*
[2]*Institut d'Astrophysique de Paris, Sorbonne Université, CNRS, UMR 7095, 98 bis Boulevard Arago, 75014 Paris, France*
[3]*Department of Physics and Astronomy, University of Louisville, Louisville, KY 40292, USA*
[4]*Gemini Observatory, 670 N. Aóhoku Place, Hilo, HI 96720, USA*
[5]*Laboratoire Interdisciplinaire Carnot de Bourgogne, Université de Bourgogne Franche Comté, CNRS, UMR 6303, F-21078 Dijon Cedex, France*
[6]*Université Gustave Eiffel, COSYS/LISIS, 5 Bd Descartes, F-77454 Champs-sur-Marne, France*
[7]*Chemistry Department, Faculty of Science, King Saud University, PO Box 2455, Riyadh 11451, Saudi Arabia*
[8]*Department of Astronomy, University of Arizona, 933 N Cherry Ave, Tucson, AZ 85719, USA*

Accepted 2020 March 10. Received 2020 March 10; in original form 2019 May 11

ABSTRACT

The spectra of helium-dominated white dwarf stars with hydrogen in their atmosphere present a distinctive broad feature centred around 1160 Å in the blue wing of the Lyman α line. It is extremely apparent in WD 1425+540 recently observed with *Hubble Space Telescope* (*HST*) Cosmic Origins Spectrograph (COS). With new theoretical line profiles based on ab initio atomic interaction potentials we show that this feature is a signature of a collision-induced satellite due to an asymptotically forbidden transition. This quasi-molecular spectral satellite is crucial to understanding the asymmetrical shape of Lyman α seen in this and other white dwarf spectra. Our previous work predicting this absorption feature was limited by molecular potentials that were not adequate to follow the atomic interactions with spectroscopic precision to the asymptotic limit of large separation. A new set of potential energy curves and electronic dipole transition moments for the lowest electronic states of the H–He system were developed to account accurately for the behaviour of the atomic interactions at all distances, from the chemical regime within 1 Å out to where the radiating H atoms are not significantly perturbed by their neighbours. We use a general unified theory of collision-broadened atomic spectral lines to describe a rigorous treatment of hydrogen Lyman α with these potentials and present a new study of its broadening by radiative collisions of hydrogen and neutral helium. These results enable ab initio modelling of radiative transport in DBA white dwarf atmospheres.

Key words: atomic data – atomic processes – line: profiles – molecular data – stars: atmospheres – white dwarfs.

1 INTRODUCTION

Theoretical studies of the effects of neutral atom collisions on atomic spectral lines have often been hindered by our ignorance of the atomic potentials. Even for systems as simple as H–H or H–He, the interactions and the electric transition moments are quite difficult to compute with the accuracy that is needed for evaluating a complete line profile. The fundamental theory of calculating the spectral line profile (Allard et al. 1999) requires knowledge of molecular potentials with high accuracy because the shape and strength of the line profile are very sensitive to the details of the molecular potential curves describing the atom–atom collisions. In Allard & Christova (2009), we made an exhaustive study of the red wing of Lyman α line perturbed by H–He collisions, where we used the potentials and electric dipole transition moments of Theodorakopoulos et al. (1984, 1987). We considered the high He densities met in cool DZ white dwarfs and examined the range of validity of the one-perturber approximation widely used to calculate the line wings. We have shown there that the extension of the red wing of the Lyman α line seen in DZ white dwarf spectra depends strongly on the stellar temperature, while it is not dependent on the helium density. We also predicted a blue satellite that only

★ E-mail: nicole.allard@obspm.fr (NFA); john.kielkopf@louisville.edu (JFK); sxu@gemini.edu (SX)

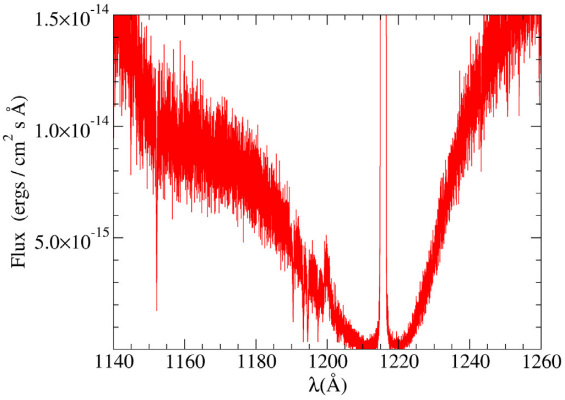

Figure 1. COS observation of WD 1425+540. The broad distinctive collision-induced satellite in the blue wing of the Lyman α line about 1160 Å is clearly visible (Xu et al. 2017). The strong emission at the centre of Lyman α is from the Earth's geocoronal hydrogen above the *HST* orbit.

very recently has been observed in *Hubble Space Telescope* (*HST*) Cosmic Origins Spectrograph (COS) observations (Xu et al. 2017). The importance of a correct determination of the blue wing of Lyman α line to interpret the asymmetrical shape of the Lyman α line observed with COS is presented in Section 2. An accurate prediction of the satellite and consequently the full Lyman α profile requires exacting new ab initio calculations to obtain the ground and first excited potential energy curves and the corresponding electric dipole transition moments for the H–He system. The new molecular data in Section 3 corroborate the prediction of a line satellite in the Lyman α profile (Allard & Christova 2009) that is described in Section 4. In Allard et al. (1999), we previously derived a classical path expression for a pressure-broadened atomic spectral line shape that includes the effects of a radiative electric dipole transition moment that is dependent on the position of the radiating atom and its dynamic neighbours. Such a comprehensive unified approach employing the precise molecular data is fundamentally necessary to obtain an accurate absorption line profile that is valid over the full breadth of spectral line for the range of densities and temperatures found in stellar atmospheres.

2 COS OBSERVATION OF WD 1425+540

WD 1425+540 ($T = 14\,490$ K, $\log g = 7.95$) is the prototype of DBA white dwarfs and it is a helium-dominated white dwarf that also has a large amount of hydrogen in its atmosphere (Bergeron et al. 2011). It was observed with *HST* COS under program 13453, and the details of observation and data reduction strategy were reported by Xu et al. (2017). Here, we focus on the spectrum of segment B of the G130M grating, which covers 1130–1270 Å, as shown in Fig. 1. As described in Xu et al. (2017), there are two unusual features of the Lyman α profile in WD 1425+540. First, the line profile is very asymmetric exhibiting an extend blue wing with the satellite feature as noted. Second, previous white dwarf spectral models cannot reproduce the strength of Lyman α and Balmer α simultaneously. The derived hydrogen abundance is more than a factor of 10 higher from the Lyman α measurement than from Balmer α. While WD 1425+540 is the most extreme case so far, these peculiarities have been observed in other DBA white dwarfs as well (e.g. Jura et al. 2012).

The asymmetry also could not be produced by white dwarf models of Xu et al. (2017) because the opacity data used for the Lyman α profile did not take into account the quasi-molecular line satellite predicted in Allard & Christova (2009). Once this feature is included, the observed asymmetry is reproduced (Gänsicke et al. 2018). The need to have both accurate data for Lyman α and for Balmer α is essential to determine the hydrogen abundance correctly. The goal of this paper is to develop the foundation of the atomic and molecular physics needed to compute a complete profile without making ad hoc assumptions. We emphasize the importance of accurate potentials and electric dipole transition moment data for this purpose, and here we provide that data for Lyman α. With new potentials of H–He we also compute a model DBA white dwarf spectrum that demonstrates their validity.

3 H–HE DIATOMIC POTENTIALS

3.1 Methodology and benchmarks

The lowest electronic excited states of hydrogen and helium are at unusually high energies for neutral atoms (>10 eV) with respect to their ground states, and close to the corresponding ionization thresholds. Hydrogen with $n = 2$ or greater is a Rydberg atom in this sense (Gallagher 1994).

The electronic excited states of H–He diatomic system of interest in this work correlate adiabatically to those of these atoms. Therefore, for the correct description of the electronic states of the H–He diatomic system consistent with its isolated atomic fragments one needs the inclusion of diffuse functions that can flexibly represent the states. In addition to this, the computation of the possible interactions that may occur between these electronic states and the subsequent mixing of their wavefunctions that results in an apparent change in electric dipole transition moments require post-Hartree–Fock multiconfigurational approaches. More specifically, we used the complete active space self-consistent field (CASSCF; Knowles & Werner 1985; Werner & Knowles 1985) followed by the internally contracted multireference configuration interaction (MRCI; Knowles & Werner 1988; Werner & Knowles 1988; Shamasundar, Knizia & Werner 2011) methods as implemented in the MOLPRO 2015 package (Werner et al. 2015). In MRCI, the complete CASSCF wavefunctions are used as a reference. Furthermore, the Davidson correction (MRCI+Q; Langhoff & Davidson 1974) has been applied to the resulting energies to account for the lack of size consistency of the MRCI method. These computations were performed in the C_{2v} point group, where the B_1 and B_2 representations were treated on equal footing.

Benchmarks on valence–Rydberg electronic states of other molecular systems (Spelsberg & Meyer 2001; Ndome et al. 2008; Hochlaf et al. 2010) showed the need to use a CASSCF active space larger than the full valence space. The atomic basis set for the H and He atoms had to be optimized as well. Thus, we performed a series of benchmark computations at different levels of accuracy to find the appropriate states for convergence.

First, at the lowest level of accuracy, we adopted a small active space of three electrons in seven molecular orbitals in conjunction with the aug-cc-pV5Z (Dunning 1989; Kendall, Dunning & Harrison 1992) basis set. With this approach, we found inconsistencies in the calculated energies, especially in the asymptotic region. Indeed, with this simplest choice there is a large energy gap of ~0.45 eV between the two equivalent dissociation limits $H(2p\,^2P) + He(1s^2\,^1S)$ and $H(2s\,^2S) + He(1s^2\,^1S)$. Obviously, this gap is unphysical since these two asymptotes should be strictly degenerate because the two H ($n = 2$) states have the same energy apart from Lamb shift and negligibly small fine and hyperfine structure. Moreover, we found a

spurious second potential well ($D_e \sim 660\,cm^{-1}$) in the $C\,\Sigma$ state of H–He at large internuclear separations (for $R_{H–He} \sim 4.2$ Å). Thus, at this level of accuracy, a rather poor chemical description of the H–He molecule is obtained in spite of the relatively large size of the MRCI computations with $\sim 4.3 \times 10^4$ uncontracted configuration state functions (CSFs) per C_{2v} symmetry. This may be linked to some missing correlation energy in the MRCI wavefunctions that can be recovered by means of larger active spaces in the reference CASSCF vector and by adopting more diffuse atomic basis sets.

Secondly, we tried an enlarged CASSCF active space of three electrons in 14 molecular orbitals in conjunction with the aug-cc-pV6Z (Dunning 1989; Kendall et al. 1992) basis set. In the subsequent MRCI treatment, the multiconfiguration wavefunctions included $\sim 2.1 \times 10^5$ uncontracted CSFs per C_{2v} symmetry. With this ansatz, the energy difference between the above-mentioned asymptotes was reduced to ∼0.33 eV but still did not vanish. For modelling based on unified spectral line shape theory an error of this size would be unacceptable.

Finally, using the same active space as in the second series of computations, we added a set of diffuse functions to the aug-cc-pV6Z basis set for H and He. Hereafter, this enlarged set will be denoted as aug-cc-pV6Z∗. The exponents of the added Gaussian primitives, which were left uncontracted, are listed in Table A1 in Appendix.

This approach, compared to the previous ones, solved all the inconsistencies mentioned above. That is, it yielded degenerate $H(2p\,^2P) + He(1s^2\,^1S)$ and $H(2s\,^2S) + He(1s^2\,^1S)$ dissociation limits and no spurious potential well in the $C\,\Sigma$ state. We note that convergence was reached at this step since a further expansion of the aug-cc-pV6Z∗ set by inclusion of more diffuse functions led to almost identical results. In these calculations, the MRCI wavefunctions included more than 7.5×10^5 uncontracted CSFs per C_{2v} symmetry species. These relatively large computations for such a small molecular system were necessary to obtain the precision needed to model the Lyman α profile accurately.

3.2 Potential energy curves and transition moments

The electronic states investigated in the present contribution correlate, at large internuclear distances, to the $H(1s\,^2S) + He(2s^2\,^1S)$, $H(2s\,^2P) + He(2s^2\,^1S)$, and $H(2p\,^2P) + He(2s^2\,^1S)$ dissociation limits (see Fig. 2 and Table A2 in Appendix). The MRCI+Q/aug-cc-pV6Z∗ potential energy curves of the four lowest electronic states of H–He, obtained with the largest active space and basis set as described in the previous section, are represented in Fig. 2 as a function of the internuclear distance, $R_{H–He}$. This figure shows that the ground state possesses a repulsive potential correlating to the $H(1s\,^2S) + He(1s^2\,^1S)$ isolated atom asymptote at large distances.

The ground $X\,^2\Sigma^+$ state is repulsive at short range with a shallow well at 4 Å. The excited $A\,^2\Sigma^+$, $B\,^2\Pi$, and $C\,^2\Sigma^+$ states have rather deep potential wells in the molecular region closer than 1 Å, and complex behaviour at longer range that can affect transition probabilities and difference potential energies in subtle ways. We refer to these as the $X\,\Sigma$, $A\,\Sigma$, $B\,\Pi$, and $C\,\Sigma$ states, or more succinctly by the letter designations X, A, B, and C in the following. They correlate adiabatically to the $H(n=2) + He(1s^2\,^1S)$ dissociation limits at large internuclear separations (see Table A2 in Appendix). The ordering of the assignments of labels for the states is with $A\,\Sigma$ the lowest and $C\,\Sigma$ the highest inside this close 1 Å region with wells in all the states of the order of $15\,000\,cm^{-1}$ deep, with minima located at $R_{H–He} = 0.7407$, 0.7686, and 0.8095 Å for

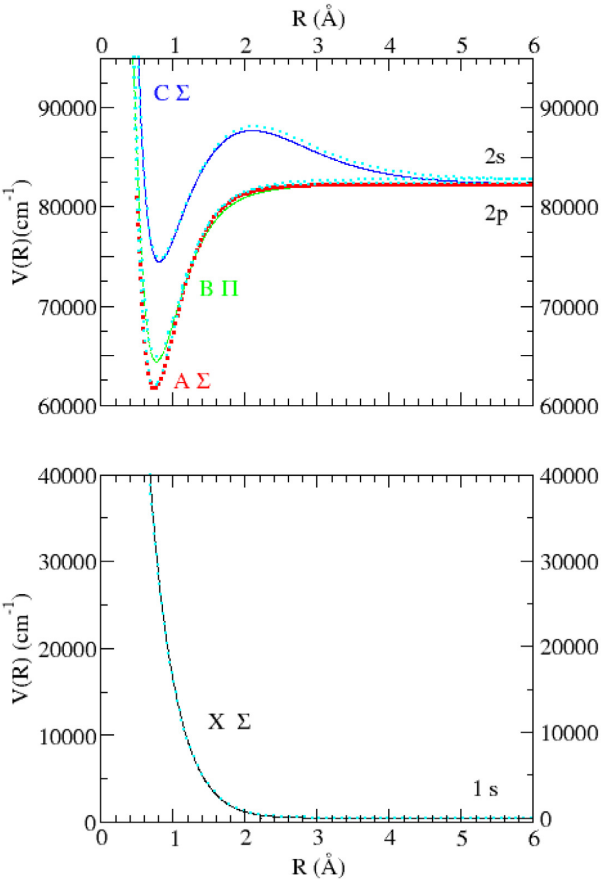

Figure 2. Top: short-range part of the potential curves of the H–He molecule: A (red dotted), B (green dashed line), and C (blue solid). Bottom: X (black solid). Note the agreement at short distance with data of Theodorakopoulos et al. (1984) that are overplotted in dotted cyan.

the A, B, and C states, respectively (see Table A3 in Appendix). While the A and B states have potentials with a simple short-range well, the C state also exhibits a potential maximum of ≈0.666 eV at $R_{H–He} = 2.098$ Å. Its presence causes a related maximum in the C–X transition difference potential energy curve that affects the blue wing of Lyman α.

Although the $C\,\Sigma$ H–He molecular state shown in Fig. 2 is correlated asymptotically with the 2s atomic state, we find that at $R_{H–He} < 7$ Å the transition probability to the $X\,\Sigma$ ground state is not zero. Detailed electric dipole transition moments between the $X\,\Sigma$ ground state and the $A\,\Sigma$, $B\,\Pi$, and $C\,\Sigma$ excited states as a function of the internuclear distance have been calculated at the MRCI/aug-cc-pV6Z∗ level. In this calculation almost all the transition moments are rather large, particularly for the $C\,\Sigma \leftarrow A\,\Sigma$ and $B\,\Pi \leftarrow A\,\Sigma$ transitions, where corresponding matrix elements of around −9.2 and −7.5 debye (D; or 10^{-18} statC cm) are calculated, respectively. Fig. A1 in Appendix offers a detailed view. These transition moments correlate to the correct atomic values at dissociation. In particular, the $\langle X\,\Sigma|DM|C\,\Sigma\rangle$ matrix element of the electric dipole transition moment (DM) vanishes at large $R_{H–He}$, where the 1s–2s transition in the isolated hydrogen atom is forbidden to one-photon electric dipole transitions by parity conservation.

4 LYMAN α OPACITY

The theory of spectral line shapes, especially the unified approach we developed, determines the contributions of specific spectral lines

to stellar opacities and may be incorporated into stellar atmosphere models to make accurate synthesis of stellar spectra possible. The line shape theory accounts for neutral atom broadening and shift in both the centres of spectral lines and their extreme wings with one consistent treatment without ad hoc assumptions about the line shape or potentials. Complete details and the derivation of the theory are provided by Allard et al. (1999). The spectrum, $I(\Delta\omega)$, is the Fourier transform (FT) of an electric dipole transition autocorrelation function, $\Phi(s)$. For a perturber density $n_{\rm p}$, we have

$$\Phi(s) = {\rm e}^{-n_{\rm p} g(s)}, \tag{1}$$

where the decay of the autocorrelation function with time leads to atomic line broadening (see equation 121 of Allard et al. 1999). Our approach introduces the concept of a modulated electric dipole transition moment $\tilde{d}_{\rm if}(R(t))$ into the line shape calculation:

$$\tilde{d}_{\rm if}[R(t)] = d_{\rm if}[R(t)]\, {\rm e}^{-\frac{V_{\rm i}[R(t)]}{2kT}}, \tag{2}$$

where the potential energy for the initial state is

$$V_{\rm i}(R) = E_{\rm i}(R) - E_{\rm i}^{\infty}. \tag{3}$$

The difference potential energy $\Delta V(R)$ for a transition 'if' is

$$\Delta V(R) = V_{\rm if}(R) = V_{\rm f}(R) - V_{\rm i}(R). \tag{4}$$

The Boltzmann factor ${\rm e}^{-\frac{V_{\rm i}(R)}{2kT}}$ in equation (2) appears because the perturbing atoms or ions are in thermal equilibrium with the radiating atom that affects the probability of finding them initially at a given R. This treatment results in Lyman series line wing profiles that exhibit a sensitive dependence on temperature. We had to use electric dipole moments modulated by the Boltzmann factor in the comparison of emission spectra of Lyman α (Kielkopf & Allard 1998) and Balmer α (Kielkopf, Allard & Decrette 2002) measured in laboratory.

4.1 Study of the characteristics of the line satellite

In Allard & Christova (2009), we predicted a line satellite at 1157 Å in spectra computed for the temperature range of cool DZ white dwarfs with potentials published in Theodorakopoulos et al. (1984). However, we noticed an unexpected well of about 150 cm^{-1} (Fig. 3, upper panel) in the potential energy of the $C\ \Sigma$ state at $R \sim 8$ Å that may be related to the choice of basis states and has no clear physical origin. In this work, we use the new ab initio calculations of the potentials over the full range of distances R between the H and He atoms since convergence at large R is now reached. The long range well of the $C\ \Sigma$ state of Theodorakopoulos et al. (1984, 1987) potentials is not found in these new calculations as we see in Fig. 3.

The prediction of a satellite in the blue wing of the H–He line profile is related to a potential maximum at $R = 2.1$ Å (see Section 3.2) of the $C\ \Sigma$ state. This leads to a maximum of the potential energy difference $\Delta V(R)$ in equation (4) for this transition shown in Fig. 3.

The unified theory predicts that line satellites will be centred periodically at frequencies corresponding to integer multiples of the extrema of $\Delta V(R)$. In the quasi-static limit the first satellite on the line would be at $\Delta\omega = 5000$ cm^{-1} corresponding to $\lambda \sim 1150$ Å on the blue side of Lyman α. In this case the maximum in ΔV occurs at rather small internuclear distance, and is quite sharp. The correspondingly short duration of the close collision leads to a broad satellite centred at $\lambda \sim 1160$ Å for $T = 14\,500$ K (Fig. 4).

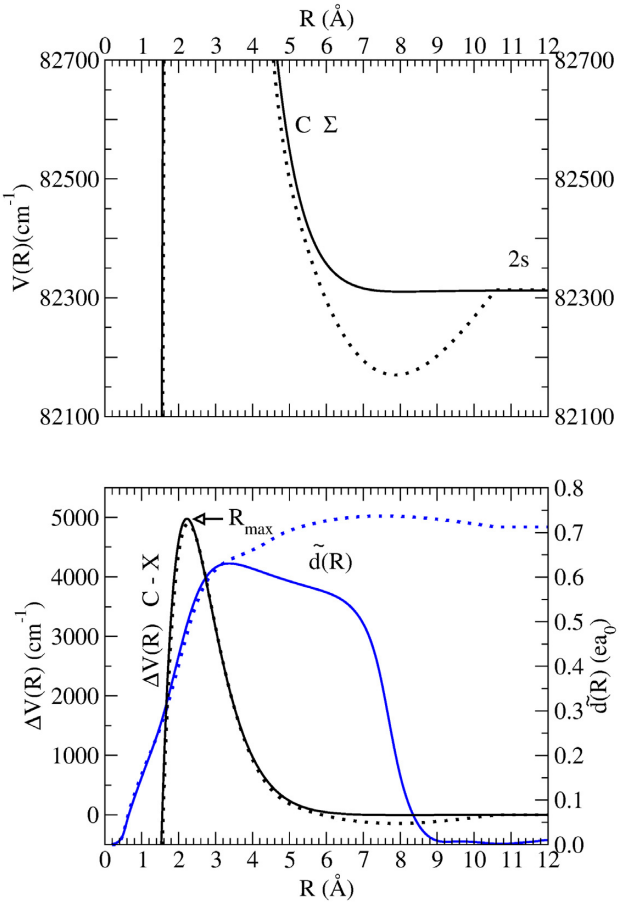

Figure 3. Top: long range part of the $C\ \Sigma$ potential curve correlated with 2s state. This work (full line); Theodorakopoulos et al. (1984) (dotted line). Bottom: $\Delta V(R)$ (black) and $\tilde{d}(R)$ (blue) at 14 500 K for the C–X transition. The atomic separation for the maximum in the C–X difference potential is $R_{\rm max} \approx 2.2$ Å as shown in Fig. 4. Note that the C–X transition in this work is forbidden asymptotically as it is a transition between the 2s and 1s states of the free hydrogen atom at large R.

4.2 Temperature and density dependence

For a lower temperature, $T = 5000$ K (Fig. 4), the duration of the collision is longer, and the line satellite at $\lambda \sim 1153$ Å is sharper and closer to the predicted quasi-static position than at higher temperatures. The oscillations that appear on the red side of the quasi-molecular satellite are due to interference effects described by Royer (1971) and Sando & Wormhoudt (1973). They depend on the relative velocity and therefore on temperature. Consequently velocity averaging would moderate their amplitude in observed spectra. At temperatures below 10 000 K the blue wing of Lyman α shortward of 1150 Å becomes significantly more transparent than at higher temperature, an order of magnitude effect below 1120 Å. Thus this far blue wing is a sensitive indicator of temperature in cool helium-rich white dwarf atmospheres.

The satellite amplitude depends on the value of the electric dipole transition moment through the region of the potential extremum responsible for the satellite and on the position of this extremum. The blue line wings shown in Fig. 4 are unchanged in the range 14 500–20 000 K as there is no change with T of $\tilde{d}_{\rm if}[R(t)]$ in the internuclear distance where the potential difference goes through a maximum. $\tilde{d}_{\rm if}[R(t)]$ at 14 500 K for the C–X transition is also plotted in Fig. 3. In the former work, we used electric dipole

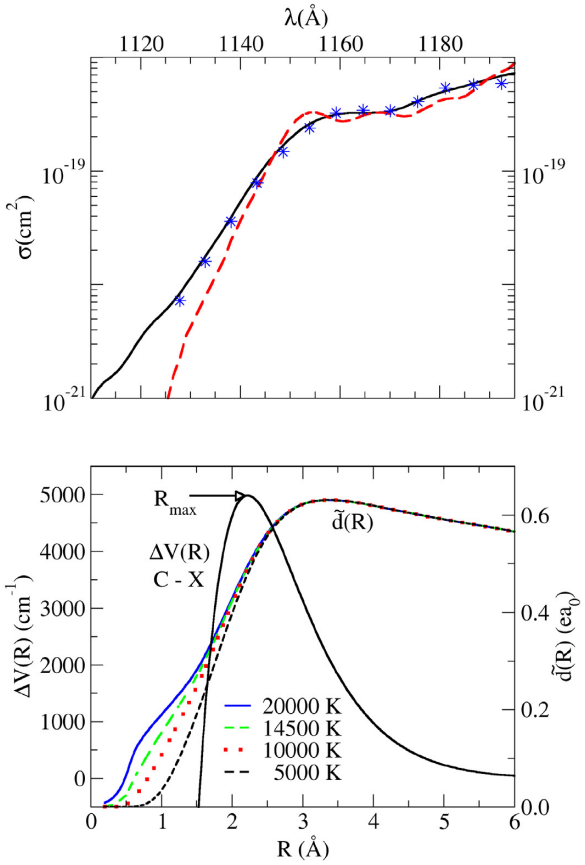

Figure 4. Top: variation with temperature of the line satellite. The He density is 1×10^{20} cm^{-3}, the temperatures are 14 500 K (full black line), 20 000 K (blue stars), and 5000 K (red dashed line). Bottom: for the C–X transition, $\Delta V(R)$ (black solid) and $d(\tilde{R})$ at 5000 K (black solid), 10 000 K (red dotted), 14 500 K (green dashed), and 20 000 K (blue solid). At the highest temperatures the He can reach the inner regions of the lower state $X\,^2\Sigma$ potential and enhance the transition probability.

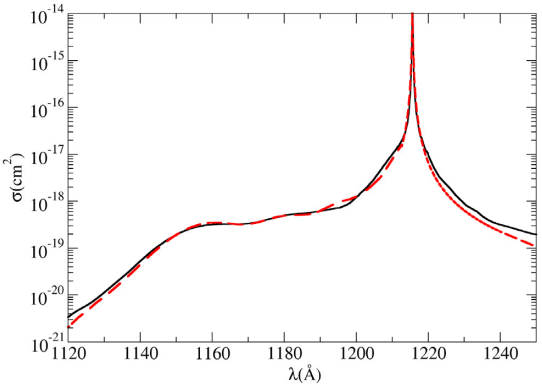

Figure 5. Comparison of the unified line profile using the dipole moments of this work (black line) with the line profile using dipole moments of Theodorakopoulos et al. (1987) (red dashed line). The He density is 10^{20} cm^{-3} and the temperature is 14 500 K.

transition moments of Theodorakopoulos et al. (1987) where the C–X transition was allowed. Nevertheless, the amplitude and position of the line satellite are unchanged as they are due to a range of internuclear distance where the potentials and the dipole moments are almost identical as we see in Fig. 5. The main difference between the two potentials concerns the red wing that is lowered using dipole moments of Theodorakopoulos et al. (1987) where the A–X transition was forbidden.

In summary the unified line profile calculation leads to a flat blue wing due to a line satellite. The resulting asymmetry of the Lyman α line can be easily appreciated in Fig. 5 the blue side of the line is wider than the red side. Measured at the strength of the broad collision-induced 1160 Å satellite, the asymmetry ratio of the width on the blue side to that on the red is as large as 2.2. Consequently, the near wing is clearly far different from a symmetric Lorentzian because the satellite is rather close to the isolated atom line centre. This was also the case for the Mg b triplet perturbed by He (Allard et al. 2016). The existence of the asymmetrical shape of these line profiles depends strongly on the maximum value of the potential energy difference $\Delta V(R)$ that predicts the position of the line satellite and on the atomic collision energies at the temperatures of interest. These results enable computing atmosphere models and synthetic spectra that we compare to an *HST* COS observation of WD 1425+540 in Section 5.

5 MODEL ATMOSPHERE AND SYNTHETIC WHITE DWARF SPECTRUM

To demonstrate the importance of a proper treatment of He perturbers on hydrogen lines, synthetic spectra of the white dwarf WD 1425+540 were computed using the stellar atmosphere code TLUSTY (version 207) for computing the atmospheric structure, and a companion program SYNSPEC (version 53) for generating detailed synthetic spectra. For a description of the previous versions (205 and 51), see the works of Hubeny & Lanz (2017) and Hubeny & Lanz (2011a,b). This procedure allows us to study the effect of the H/He ratio on the spectrum, and the development of line wings, though it is not fully self-consistent with the stellar atmosphere model since that would require a treatment of He I optical lines as well. We have computed a number of H–He models, with the basic model parameters, $T_{\rm eff} = 14\,410$ K and $\log g = 7.89$, from Gänsicke et al. (2018), and with varying He/H ratio. For treating the electron and proton broadening of the hydrogen lines we used Tremblay & Bergeron (2009) data. The He/H ratio was adjusted to obtain a reasonable agreement by eye with the observed spectrum, and we found a nominal ratio of 4×10^3 ($\log(N_{\rm H}/N_{\rm He}) \approx -3.6$) fitted the observed profile well. Liebert et al. (1979) found 3.7 from a ground-based Hβ profile, and recently Gänsicke et al. (2018) analysed the Lα profile and adopted a somewhat larger $\log(N_{\rm H}/N_{\rm He}) \approx -4.0 \pm 0.20$.

The potential energies for the $n = 1$ and $n = 2$ electronic states H–He that were used in our models are the ones described in this paper. Stellar opacities were computing using H–He electric dipole moments from the previous work of Theodorakopoulos et al. (1987) in which the A–X transition is forbidden, and also using new dipole transition moments from this work in which the A–X transition is allowed. As shown in Fig. 6, the observed red wing of Lyman α is consistent with a suppressed A–X transition probability in the region of atomic separation with difference potential energy that would contribute.

We conclude that the additional basis states used for the new ab initio potentials improve the calculation of the potential energy curves, but may not capture the dipole transition moments of the real H–He system correctly for the A–X transition. However, the combination of this work's potentials and the dipole moments of Theodorakopoulos et al. (1987) achieve a remarkable fit in Fig. 6 to the *HST* COS spectrum of WD 1425+540 when incorporated into the unified line shape theory we described here.

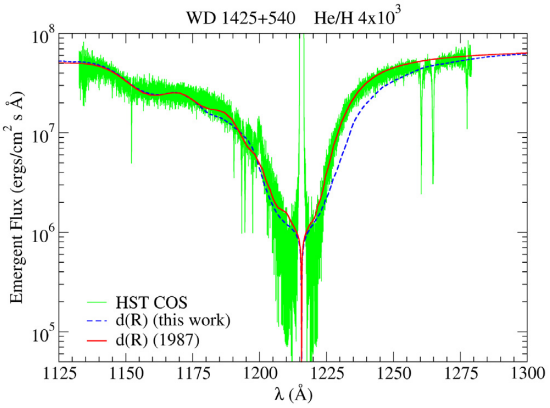

Figure 6. The observed spectrum of WD 1425+540 (also see Fig. 1) compared with a synthetic white dwarf spectrum in the Lyman α region. The synthetic spectrum is computed with TLUSTY and SYNSPEC for a temperature of 14 500 K and a He/H ratio of 4×10^3 using the unified line profile with the potentials of this work. For the dipole moments of Theodorakopoulos et al. (1987) (red solid line), the A–X transition is forbidden and its contributions to the opacity are suppressed. For the dipole moments of this work (blue dashed line), the A–X transition contributes in the red wing of the model but is absent in the observed spectrum.

6 CONCLUSIONS

The Lyman α region of the spectrum of a helium-rich white dwarf with hydrogen in its atmosphere is determined by the changes in transition energy and transition probability during the H–He collisions that broaden the atomic spectral line. We developed new H–He potential energies and transition dipole moments for the hydrogen 1s, 2s, and 2p states as input data for a unified theory calculation of the profile of WD 1425+540 to test the potentials and dipole moments, and to confirm the origin of the short-wavelength 'blue' satellite. We found that the spectral line profile from the new molecular data has a satellite feature in the blue wing that agrees with previous work. These results provide a benchmark implementation of ab initio atomic and molecular potentials for the most basic neutral non-resonant atom–atom pair relevant to stellar atmosphere models. The new calculations show how the profile depends on the variation of the electric dipole transition moment and interaction potential energy with atomic separation. A comparison with the observed spectrum of WD 1425+540 was made by using these theoretical opacities in a stellar atmosphere and spectrum synthesis code. While it was not our goal to refine the stellar model based on the new theoretical data, the profiles reproduce the observed spectrum with a reasonable He/H ratio. Further, the absence of an extended red wing of Lyman α in the observed spectrum suggests that the states of the difference potential that could contribute to that region have the reduced transition dipole moment that was found in previous molecular models. The new work presented here shows clearly that there is an opportunity to use stellar spectra to improve the atomic and molecular physics, ultimately to yield better models for astrophysical applications. For H–He, the A–X transition dipole moment remains uncertain.

The blue wing of Lyman α is sensitive to He density and the structure and temperature of the stellar atmosphere, with a profile that for wavelengths shortward of 1150 Å will have reduced opacity from regions with temperatures under 10 000 K. Profiles computed with a unified theory of collision broadening based on accurate data from ab initio molecular physics take into account the strong dependence of the amplitude of the electric dipole transition moment on atom–atom separation (R) where the potential energy change $\Delta V(R)$ is an extremum. Incorporated into model atmospheres, this dependence may be used to probe white dwarf or stellar atmospheres for density and temperature. This emphasizes the importance of the accuracy of both the potential energies and the electric dipole transition moments for the line shape calculations that have traditionally assumed electric dipole transition moments are constant (Allard & Kielkopf 1982; Allard & Koester 1992; Allard et al. 1994).

The effect of collision broadening is central to understanding the opacity of stellar atmospheres, yet there have been only a few definitive comparisons with experimental work for atomic H (Kielkopf & Allard 1995, 1998; Kielkopf, Allard & Huber 2004). This is because of the difficulty of creating an environment in a laboratory experiment simulating a stellar atmosphere with accurate diagnostics. On the theoretical side, the maturing capability of ab initio methods now offers the possibility of accurately computing the interaction of H with H (Drira 1999; Spielfiedel 2003; Spielfiedel, Palmieri & Mitrushenkov 2004) and H with He atoms (this work). While an accurate determination of the broadening of Balmer α with high density atomic hydrogen (i.e. H–H) has been done by Allard et al. (2008), nothing comparable exists for H–He. Our calculations reported in Allard et al. (2008) support the results of Barklem, Piskunov & O'Mara (2000), Barklem et al. (2002) that the Ali & Griem (1966) theory underestimates the actual line width. Recent laboratory measurements show a similar result at high density in environments comparable to white dwarf atmospheres (Kielkopf & Allard 2014). It would be possible now to similarly improve the calculation of Balmer α broadening and its contribution to the full white dwarf opacity model. A major improvement to comprehensive theoretical models for DBA white dwarf spectra is within reach that would determine H–He molecular data for $n = 3$ excited states, and use those to compute accurate Balmer α profiles under white dwarf atmosphere conditions. Such results would help understanding the differences in stellar parameters that are found from Balmer and Lyman line profiles. In conclusion, complete unified line profiles based on accurate atomic and molecular physics for both the Lyman α and Balmer α lines should be incorporated into the analysis of DBA white dwarf spectra to derive the hydrogen abundance.

ACKNOWLEDGEMENTS

This paper is based on observations made with the NASA/ESA *Hubble Space Telescope* under program 13453, obtained from the data archive at the Space Telescope Science Institute (STScI). STScI is operated by the Association of Universities for Research in Astronomy, Inc. under NASA contract NAS 5-26555. We thank the COST Action CM1405 MOLecules in Motion (MOLIM) of the European Community for support. The authors would like to extend their sincere appreciation to the Deanship of Scientific Research, King Saud University for funding the research through the Research Group Project No. RGP-333. This work was supported by the CNRS program Physique et Chimie du Milieu Interstellaire (PCMI) cofunded by the Centre National d'Etudes Spatiales (CNES).

REFERENCES

Ali A. W., Griem H. R., 1966, Phys. Rev., 144, 366
Allard N. F., Christova M., 2009, New Astron. Rev., 53, 252
Allard N. F., Kielkopf J. F., 1982, Rev. Modern Phys., 54, 1103
Allard N. F., Koester D., 1992, A&A, 258, 464

Allard N. F., Koester D., Feautrier N., Spielfiedel A., 1994, A&AS, 108, 417
Allard N. F., Royer A., Kielkopf J. F., Feautrier N., 1999, Phys. Rev. A, 60, 1021
Allard N. F., Kielkopf J. F., Cayrel R., van 't Veer-Menneret C., 2008, A&A, 480, 581
Allard N. F., Leininger T., Gadéa F. X., Brousseau-Couture V., Dufour P., 2016, A&A, 588, A142
Barklem P. S., Piskunov N., O'Mara B. J., 2000, A&A, 363, 1091
Barklem P. S., Stempels H. C., Allende Prieto C., Kochukhov O. P., Piskunov N., O'Mara B. J., 2002, A&A, 385, 951
Bergeron P. et al., 2011, ApJ, 737, 28
Drira I., 1999, J. Mol. Spectrosc., 198, 52
Dunning T. H., Jr, 1989, J. Chem. Phys., 90, 1007
Gallagher T. F., 1994, Rydberg Atoms. Cambridge Univ. Press, Cambridge
Gänsicke B. T., Koester D., Farihi J., Toloza O., 2018, MNRAS, 481, 4323
Hochlaf M., Ndome H., Hammoutène D., Vervloet M., 2010, J. Phys. B: At. Mol. Opt. Phys., 43, 245101
Hubeny I., Lanz T., 2011a, Astrophysics Source Code Library, record ascl:1109.021
Hubeny I., Lanz T., 2011b, Astrophysics Source Code Library, record ascl:1109.022
Hubeny I., Lanz T., 2017, preprint (arXiv:1706.01859)
Jura M., Xu S., Klein B., Koester D., Zuckerman B., 2012, ApJ, 750, 69
Kendall R. A., Dunning T. H., Jr, Harrison R. J., 1992, J. Chem. Phys., 96, 6796
Kielkopf J. F., Allard N. F., 1995, ApJ, 450, L75
Kielkopf J. F., Allard N. F., 1998, Phys. Rev. A, 58, 4416
Kielkopf J. F., Allard N. F., 2014, J. Phys. B: At. Mol. Opt. Phys., 47, 155701
Kielkopf J. F., Allard N. F., Decrette A., 2002, European Phys. J. D, 18, 51
Kielkopf J. F., Allard N. F., Huber J., 2004, ApJ, 611, L129
Knowles P. J., Werner H.-J., 1985, Chem. Phys. Lett., 115, 259
Knowles P. J., Werner H.-J., 1988, Chem. Phys. Lett., 145, 514
Kramida A. E., 2010, At. Data Nucl. Data Tables, 96, 586
Langhoff S. R., Davidson E. R., 1974, J. Quant. Chem., 8, 61
Liebert J., Gresham M., Hege E. K., Strittmatter P. A., 1979, AJ, 84, 1612
Ndome H., Hochlaf M., Lewis B. R., Heays A. N., Gibson S. T., Lefebvre-Brion H., 2008, J. Chem. Phys., 129, 164307
Royer A., 1971, Phys. Rev. A, 4, 499
Sando K. M., Wormhoudt J. G., 1973, Phys. Rev. A, 7, 1889
Shamasundar K. R., Knizia G., Werner H.-J., 2011, J. Chem. Phys., 135, 054101
Spelsberg D., Meyer W., 2001, J. Chem. Phys., 115, 6438
Spielfiedel A., 2003, J. Mol. Spectrosc., 217, 162
Spielfiedel A., Palmieri P., Mitrushenkov A., 2004, Mol. Phys., 102, 2249
Theodorakopoulos G., Farantos S. C., Buenker R. J., Peyerimhoff S. D., 1984, J. Phys. B: At. Mol. Opt. Phys., 17, 1453
Theodorakopoulos G., Petsalakis I. D., Nicolaides C. A., Buenker R. J., 1987, J. Phys. B: At. Mol. Opt. Phys., 20, 2339
Tremblay P. E., Bergeron P., 2009, ApJ, 696, 1755
Werner H.-J., Knowles P. J., 1985, J. Chem. Phys., 82, 5053
Werner H.-J., Knowles P. J., 1988, J. Chem. Phys., 89, 5803
Werner H.-J. et al., 2015, MOLPRO, version 2015.1, a package of *ab initio* programs (see http://www.molpro.net)
Xu S., Zuckerman B., Dufour P., Young E. D., Klein B., Jura M., 2017, ApJ, 836, L7

APPENDIX

Parameters of the H–He molecular potentials are given in Tables A1 and A2. Fig. A1 shows the dependence on R of the radiative transition moments between the excited states and the perturbations of those states as the H and He atoms approach from large R.

Table A1. Exponents of the diffuse uncontracted Gaussian primitives added to the aug-cc-pV6Z basis set to form the presently used aug-cc-pV6Z∗ basis sets for the H and He atoms.

State	1	2	3
H(s)	0.00690204	0.002520537	0.000920468
H(p)	0.026565598	0.010533298	0.004176468
H(d)	0.055406537	0.024364162	0.010713761
H(f)	0.106396067	0.046204584	0.020065249
H(g)	0.168703345	0.069928301	0.028985598
H(h)	0.175320015	0.045069073	0.011585793
He(s)	0.017177900	0.006596920	0.002533450
He(p)	0.050416903	0.019858313	0.007821833
He(d)	0.094209988	0.036827891	0.014396494
He(f)	0.151890237	0.056684629	0.021154402
He(g)	0.232902520	0.079072280	0.026845675
He(h)	0.248198125	0.060632194	0.014811808

Table A2. Dissociation fragments, experimental and calculated relative dissociation asymptotic energies, and molecular states for the four lowest electronic states of H–He. Experimental data are from Kramida (2010).

Atomic		Observed	Calculated	Molecular
H	He	(cm^{-1})	(cm^{-1})	
$1s\,^2S_g$	$1s^2\,^1S_g$	0^a	0^a	$X\,^2\Sigma^+$
$2p\,^2P_u$	$1s^2\,^1S_g$	82259	82308	$A\,^2\Sigma^+$, $B\,^2\Pi$
$2s\,^2S_g$	$1s^2\,^1S_g$	82259	82308	$C\,^2\Sigma^+$

[a]Reference.

Table A3. Spectroscopic constants and dissociation energies for the three lowest excited electronic states of H–He as deduced from the MRCI+Q /aug-cc-pV6Z∗ potential energy curves. R_e corresponds to the equilibrium distance. ω_e and $\omega_e x_e$ are the vibrational constants. β_e and α_e are the rotational constants. D_e is the dissociation energy.

State	R_e (Å)	ω_e (cm^{-1})	$\omega_e x_e$ (cm^{-1})	β_e (cm^{-1})	α_e (cm^{-1})	D_e (eV)
$A\,^2\Sigma^+$	0.74074	3697.2	149.5	38.16	2.608	2.563
$B\,^2\Pi$	0.76863	3313.4	149.8	35.44	2.629	2.218
$C\,^2\Sigma^+$	0.80953	2906.3	144.0	31.95	2.551	1.638

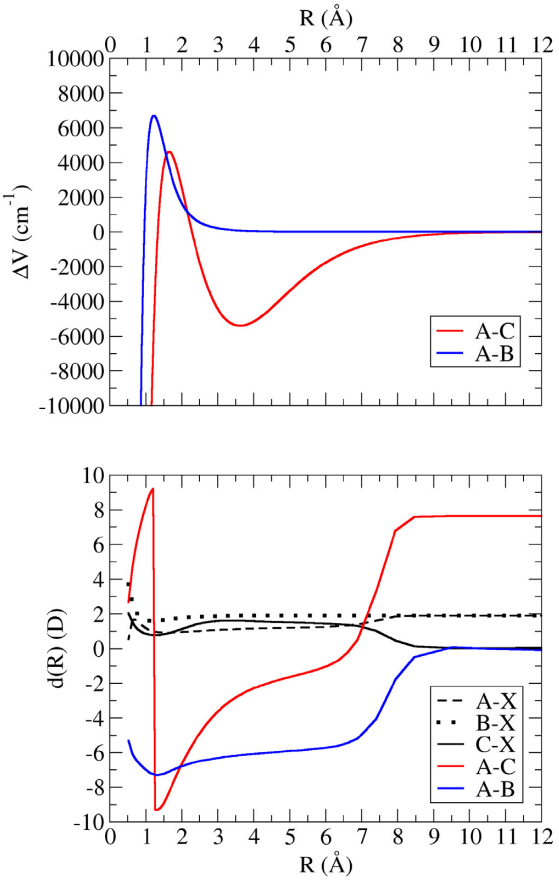

Figure A1. Potential energy differences in cm^{-1} and electric dipole transition moments in debye (D; or 10^{-18} statC cm) between the four lowest electronic states of H–He calculated at the MRCI/aug-cc-pV6Z* level. Note that the $C\,\Sigma \leftarrow X\,\Sigma$ is asymptotically forbidden, while transitions between excited states may occur. Upper panel: energy differences $A\Sigma - B\Sigma$ (blue) and $A\Sigma - C\Pi$ (red). Lower panel: electric dipole transition moments for H in the presence of He for states contributing to H Lyman α.

This paper has been typeset from a TEX/LATEX file prepared by the author.